Protoporphyrin IX fluorescence contrast in invasive glioblastomas is linearly correlated with Gd enhanced magnetic resonance image contrast but has higher diagnostic accuracy

Kimberley S. Samkoe
Summer L. Gibbs-Strauss
Harold H. Yang
S. Khan Hekmatyar
P. Jack Hoopes
Julia A. O'Hara
Risto A. Kauppinen
Brian W. Pogue

Protoporphyrin IX fluorescence contrast in invasive glioblastomas is linearly correlated with Gd enhanced magnetic resonance image contrast but has higher diagnostic accuracy

Kimberley S. Samkoe,[a,b] Summer L. Gibbs-Strauss,[a] Harold H. Yang,[a] S. Khan Hekmatyar,[c] P. Jack Hoopes,[a,b] Julia A. O'Hara,[a,c] Risto A. Kauppinen,[c] and Brian W. Pogue[a,b]
[a]Dartmouth College, Thayer School of Engineering, Hanover New Hampshire 03755
[b]Dartmouth Medical School, Department of Surgery, Lebanon, New Hampshire 03756
[c]Dartmouth Medical School, Department of Diagnostic Radiology, Hanover, New Hampshire 03755

Abstract. The sensitivity and specificity of *in vivo* magnetic resonance (MR) imaging is compared with production of protoporphyrin IX (PpIX), determined *ex vivo*, in a diffusely infiltrating glioma. A human glioma transfected with green fluorescent protein, displaying diffuse, infiltrative growth, was implanted intracranially in athymic nude mice. Image contrast from corresponding regions of interest (ROIs) in *in vivo* MR and *ex vivo* fluorescence images was quantified. It was found that all tumor groups had statistically significant PpIX fluorescence contrast and that PpIX contrast demonstrated the best predictive power for tumor presence. Contrast from gadolinium enhanced T1-weighted (T1W + Gd) and absolute T2 images positively predicted the presence of a tumor, confirmed by the GFP positive (GFP+) and hematoxylin and eosin positive (H&E+) ROIs. However, only the absolute T2 images had predictive power from controls in ROIs that were GFP+ but H&E negative. Additionally, PpIX fluorescence and T1W + Gd image contrast were linearly correlated in both the GFP+ ($r = 0.79$, $p<1\times10^{-8}$) and H&E+ ($r = 0.74$, $p<0.003$) ROIs. The trace diffusion images did not have predictive power or significance from controls. This study indicates that gadolinium contrast enhanced MR images can predict the presence of diffuse tumors, but PpIX fluorescence is a better predictor regardless of tumor vascularity. © *2011 Society of Photo-Optical Instrumentation Engineers (SPIE)*. [DOI: 10.1117/1.3622754]

Keywords: protoporphyrin IX; aminolevulinic acid; glioblastoma; fluorescence-guided resection; magnetic resonance imaging.

Paper 11218R received May 4, 2011; revised manuscript received Jul. 15, 2011; accepted for publication Jul. 18, 2011; published online Sep. 1, 2011.

1 Introduction

High-grade gliomas are aggressive tumors that are difficult to fully resect due to their infiltrative nature and diffuse tumor margins. The introduction of the aminolevulinic acid (ALA)–protoporphyrin IX (PpIX) system has found great success clinically in fluorescence guided resection (FGR) for minimizing the amount of malignant glioma tissue remaining in the patient post-surgical resection in Germany,[1–6] and is ongoing in clinical trials in the United States[7–10] and Switzerland.[11] Current standard of care for brain cancer patients undergoing surgery includes magnetic resonance (MR) imaging prior to surgery to map tumor extent, surgical resection, and post-surgical MR imaging to determine if any contrast-enhancing tumor region remains. However, tumor margins determined from conventional MR imaging [gadolinium (Gd) enhanced T1-weighted] and PpIX fluorescence often do not agree,[1] even with advanced algorithms to account for brain deformation during the surgical intervention.[8] This paper evaluates the correlation between tissue contrast from PpIX fluorescence and Gd-enhanced T1-weighted, absolute T2, and diffusion MR images using a highly infiltrative human glioma in a murine model.

The ALA–PpIX system provides tumor to normal tissue contrast through production of PpIX in malignant tissues following ALA administration by overwhelming the heme biosynthesis pathway, found in all mammalian cells.[12] Glioma tissues produce higher levels of PpIX as compared to normal brain tissues for a range of reasons, including increased vascular permeability, increased cellular metabolism, and a modified tumor microenvironment.[12] It is not well established what level of compromise to the blood-brain-barrier (BBB) will lead to ALA infiltration; however, it is well known that the highest levels of PpIX are found within glioma tissue, regions of inflammation, and structures not associated with the BBB (i.e., meninges and choroid plexus).[13]

Surgical resection of gliomas is based on tumor boundaries determined by conventional Gd contrast enhanced (MR) imaging. However, intratumoral heterogeneity, including solid tumor, necrosis, tumor infiltration, and edema, of glioma tumors is not always recognizable in conventional MR imaging.[14] In an initial FGR study Stummer et al.[1] noted that residual PpIX fluorescence after FGR was observed in 35 patients, suggesting unresected tumor had been left; yet 17 of these patients were devoid of Gd contrast enhancement in post-operative T1 weighted MR images. The discrepancy between tumor margins in MR imaging and PpIX fluorescence has also been noted before by

Address all correspondence to Kimberley Samkoe, Dartmouth College, Thayer School of Engineering, Hanover, New Hampshire 03755. Tel: (603) 646-7618; Fax (603) 646-3856; E-mail: Kimberley.Samkoe@Dartmouth.edu.

Gibbs-Strauss et al.[15] in the tumor-line U251-GFP (green fluorescent protein), which grows in a highly diffusive and scattered morphology. It was demonstrated in a U251-GFP murine model that MR image contrast from gliomas depended on the pattern of tumor growth. Diffusely growing tumors did not have as high, if any, image contrast in Gd enhanced MR images. A recent pilot study in two human cases[8] comparing pre-operative MRI to intrasurgical FGR fluorescence using a method to spatially register them, showed that there was synergy in using both methods to identify the diseased regions for resection, as assessed by sensitivity and specificity of detection.

The goal of this study was to examine this result in a murine model, and determine if there was a direct correlation between the image contrast produced by a variety of conventional (gadolinium enhanced) and nonconventional (absolute T2 and diffusion) MR images as compared to *ex vivo* fluorescence image contrast from PpIX. Additionally, furthering this goal was to determine whether PpIX had a higher positive predictive value than MR imaging for diffuse gliomas. The glioma model used is a U251-GFP cell line that was created in house,[15] and resulted in the creation of a cell line that exhibits growth patterns atypical of the parent U251 cell line.

2 Materials and Methods

2.1 Animals

All animals were used in accordance with the policies and an approved protocol of the Institutional Animal Care and Use Committee at Dartmouth College. Fifteen 6-week-old, male NCR athymic nude mice were obtained from the National Cancer Institute–Frederick Animal Production Program (Frederick, Maryland) and used in this study. There were 12 mice (9 tumor implanted, 3 sham surgery controls) that underwent MRI and PpIX study only, while an additional 3 mice were used for fluorescence staining.

2.2 Cell Culture and Murine Orthotopic Glioma Model

U251-GFP was used for implantation.[15] The U251-GFP cells were cultured in Dulbecco's Modification of Eagle's Medium (DMEM, Mediatech, Inc., Herndon, Virginia) supplemented with 10% fetal bovine serum (FBS, Mediatech, Inc.) and 1% penicillin-streptomycin (Mediatech, Inc.). The cells were incubated in a humidified environment at 37 °C with 95% air and 5% carbon dioxide. In preparation for injection, the cells were trypsinized, live cell count performed on a hemocytometer with Trypan blue to stain the dead or damaged cells, and then were subsequently suspended in phosphate buffer saline (PBS) for implantation at the appropriate concentration.

The procedure for orthotopic brain tumor implantation has been described previously, but is described briefly here. Mice were anesthetized by interperitoneal (i.p.) injection with ketamine-xylazine (90:10 mg/kg) and a small incision was created on the left side of the head exposing the skull landmarks. A small hole was created 2 mm behind the bregma and 2 mm to the left of the midline using a 1 mm rotary drill. A Hamilton syringe (Hamilton Company, Reno, Nevada) was placed 2-mm deep into the brain tissue and 1×10^6 cells in 10 μl was injected

over a 5 minute period, followed by a slow retraction of the needle to prevent cell leakage. The control mice received the same treatment, but were injected with 10 μl of PBS only. The hole in the skull was closed using bone wax (Ethicon, Inc., Piscataway, New Jersey) and the incision closed with Vetbond (J. A. Webster, Inc., Sterling, Massachusetts). All mice implanted with U251-GFP cells displayed tumor cell growth, although tumor size varied considerably due to the diffuse and infiltrative nature of the cell line as previously reported.[15, 16] Mice were imaged 10 to 16 days post-implantation when they displayed clinical signs of tumor growth.

2.3 MRI

All MR experiments were performed on a 7T/21cm magnet (Magnex Scientific, Abingdon, United Kingdom) equipped with an imaging gradient set (Resonance Research Inc, Billerica, Massachusetts), interfaced to a Varian UNITY-INOVA console (Varian Inc., Walnut Creek, California). A Litz coil of 20-mm diameter (Doty Scientific Inc, Columbia, South Carolina) was used in transmit/receive mode. The mice were anesthetized with isoflurane (1 to 1.5 vol.% in 70:30 O_2:N_2) with a nose cone, and an animal torso was placed on a thermostated water circulating heating element at 37 °C for the duration of MR scans to maintain body temperature. Pre- and post-contrast T_1 MR images were acquired with a standard spin echo sequence using the following acquisition parameters: TR = 700 ms, TE = 9 ms, matrix size = 128 × 128, field of view (FOV) = 30 × 30 mm, 2 signal averages, slice thickness = 0.75 mm, number of slices = 20, total acquisition time = 3 min 3 s. For post-contrast T_1, Magnevist (0.2 mmol/kg) was injected i.p. 10 min before acquisition of T_1 MRI. A multiecho, multislice spin echo sequence was used to acquire absolute T_2 MR images with parameters as follows: TR = 3 s, TE = 20 ms, number of echoes = 4, 2 signal averages, matrix size = 128 × 128, FOV = 30 × 30 mm, slice thickness = 0.75 mm, number of slices = 20, total acquisition time = 12 min 55 s. The trace of the diffusion images (D_{av}) was acquired using the sequence described by Mori and van Zijl[17] with acquisition parameters as follows: TR = 1.5 s, TE = 55 ms, matrix size = 128×64, FOV = 30×30 mm, 2 signal averages, slice thickness = 0.75 mm, number of slices = 15 to 20, three b-values = 0, 496.6 and 1056.7 s/mm^2, total acquisition time = 9 min 41 s. The Aedes routine (http://aedes.uku.fi) performed under a MATLAB platform (Mathworks Inc, Bolder, Colorado) was used to compute both absolute T_2 and D_{av} images from the acquired data sets.

2.4 Ex vivo Frozen Tissue Fluorescence Imaging and Histology

Post-MR imaging, the mice were administered 100 mg/kg ALA dissolved in PBS by i.p. injection. Two hours post-ALA injection, the mice were sacrificed; the brains were extracted and sectioned in the coronal plane into four pieces, ensuring that one slice was made directly through the needle track to optimize tumor detection. The sections were laid cut face down on a glass slide and were imaged on a fluorescence plate scanner (Typhoon 9410, GE Healthcare Life Sciences) for both PpIX (633-nm excitation, 650-nm LP emission) and GFP (488-nm excitation, 526-nm BP emission) fluorescence. Following fluorescence imaging the brain slices were sent to pathology

for routine H&E staining on 4 μm tissue slices. Routinely, the surface slice was kept for each tissue section and subsequent slices were taken every 100 μm throughout the entirety of the tissue. The tissue between each H&E slice was discarded at the time of preparation.

Additional fluorescence imaging on frozen sections was performed in three mice to verify compromised vasculature and blood-brain barrier breakdown as a mode of ALA delivery. In addition to the ALA administered 2 h prior to sacrifice, the mice were i.v. injected with the vascular marker Hoechst 33258 (15 mg/kg in PBS) via the tail vein 1 min prior to sacrifice. The brains were removed, submerged in Tissue Tek® Optimum Cutting Temperature medium, and flash frozen in a mixture of methylbutane and dry ice. The frozen brain samples were stored short term at $-20\,^\circ$C and long term at $-80\,^\circ$C. Ten micrometer thick frozen tissue sections were made on a cryotome (CM 1850, Leica Biosystems). Two consecutive slices were made every 100 μm throughout the entirety of the brain sample. The first slice was used for fluorescence imaging and the second slice was sent for routine H&E staining to confirm tumor location. Fluorescence imaging was performed on a Nikon DIAPHOT-TMD inverted fluorescence microscope with a QColor3 CCD camera and QCapture Suite imaging software (QImaging, Surrey, BC, Canada). GFP (ex: 470 to 490 nm, em: 520 to 560 nm; DM510, BIE filter cube, Nikon, Garden City, New York), PpIX (ex: 445 nm, em: 685 to 715 nm; 560DCXR, C36848; Chroma Technology Corp., Rockingham, Vermont), and Hoechst 33258 (ex: 360 to 370 nm, em: 425 to 475, HQ450/50m dichroic; Chroma Technology Corp.) were imaged in the same field of view for fluorescence correlation. The GFP fluorescence overlaps with Hoechst 33258 fluorescence in the 520 to 560 nm range; however, the Hoechst 33258 fluorescence could be separated using the shorter wavelength filter cube.

2.5 Contrast Analysis

Corresponding regions of interest (ROIs) for the fluorescence and MR images were produced to compare the contrast between image types. ROIs were created using *ImageJ* (Rasband, W.S., ImageJ, U.S. National Institutes of Health, Bethesda, Maryland, http://rsb.info.nih.gov/ij/, 1997 to 2005) from the GFP-fluorescence images and were copied to the PpIX images and the correlating MR image slices. The tumor location was confirmed in the H&E slices, and the ROIs were divided into two groups based on the GFP fluorescence: H&E positive (H&E+) and negative (H&E−) ROIs. The image contrast was determined using the following formula:

$$\text{Contrast} = \frac{I_{\text{ROI}} - I_{\text{Bkgd}}}{I_{\text{Contra}} - I_{\text{Bkgd}}} \qquad (1)$$

where I_{ROI} is the average pixel intensity in the region of interest, I_{Contra} is the average pixel intensity in the contralateral region of the brain, and I_{Bkgd} is the average pixel intensity in the background of the image. Thus, Contrast = 1 indicates that there is no difference between the ROI and its contralateral region, while Contrast > 1 and Contrast < 1 signifies a signal enhancement or depression, respectively, within the tumor region of interest. Student's t-test statistics with unequal variance and Pearson's correlation coefficient calculations were used to analyze the data, performed using OriginPro 8 (OriginLab, Northhampton,

Massachusetts). A variety of diagnostic tests were calculated for each imaging contrast type and ROI group, including: sensitivity, specificity, positive predictive value (PPV), negative predictive value (NPV), and diagnostic accuracy.

3 Results

3.1 Regions of Interest

The H&E slices were used to guide the location of the tumors in the GFP fluorescence images for the initial ROI determination. There were 36 ROIs that displayed GFP fluorescence (GFP+). It was readily noted that within these 36 ROIs there were distinct regions that displayed GFP fluorescence (i.e., U251-GFP cells) in the thick tissue sections used for fluorescence imaging that did not appear in the 4 μm surface H&E sections. Therefore, the paraffin embedded tissue blocks were further sectioned by taking a 4 μm slice every 100 μm for the entirety of the tissue. Although this increased the number of correlating GFP fluorescence and tumor H&E positive ROIs, there were still many that could not be correlated with H&E stained tissues. Therefore, the GFP + ROIs were further divided into two categories: H&E positive (H&E+) and H&E negative (H&E−); although the latter group is designated H&E−, it is believed that the GFP fluorescence indicates the presence of tumor. There were 36 GFP + ROIs noted in 9 mice, with 14 of those ROIs H&E+ and 22 H&E negative (H&E−). Twenty-four ROIs were created for three sham surgery control mice.

Figure 1 demonstrates a complete set of images for one representative mouse in the study. The regions of interest within the brain are denoted with arrows. Note that there are three H&E + ROIs in this particular mouse. The corresponding ROIs in the GFP and PpIX fluorescence images are shown in
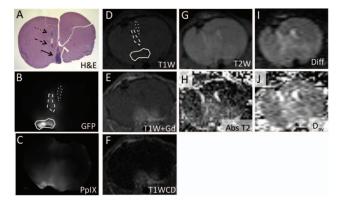

Fig. 1 The diffusely growing U251-GFP tumor images are shown using *ex vivo* fluorescence, *in vivo* MR imaging, and *ex vivo* H&E staining. (a) H&E staining of a mouse brain implanted with U251-GFP shows three regions (black arrows – dotted, dashed, and solid) of diffusely growing glioma cells. H&E was used as the gold standard for tumor detection. (b) GFP fluorescence from thick tissue slices was used to determine the ROIs for fluorescence and MR imaging contrast analysis. The three ROIs are circled with dotted, dashed, and solid lines corresponding to the ROIs indicated in (a). (c) PpIX fluorescence of the same tissue slice was analyzed. The following MR imaging scans were also analyzed for tumor contrast: (d) T1W without gadolinium contrast [dotted, dashed, and solid circles correspond to GFP fluorescence ROIs indicated in (b)], (e) T1W with gadolinium, (f) T1W contrast difference, (g) T2, (h) absolute T2, (i) diffusion, and (j) D_{av} image. The ROIs created in the MR images corresponding to fluorescence and H&E images are shown in the T1W without gadolinium image (d).
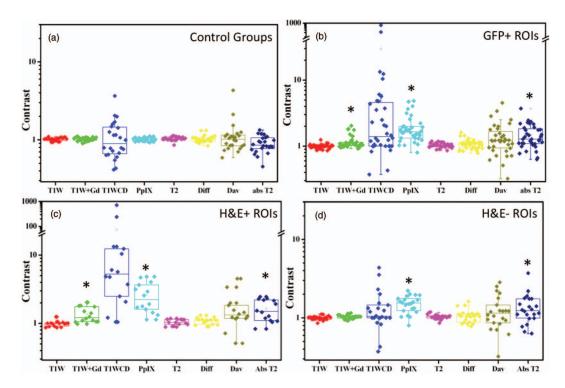
Fig. 2 The comparison of MRI and fluorescence contrast (where contrast = [ROI] / [Contralateral ROI]) of the control mice (a), and the GFP + ROIs (b) show that the T1W + Gd, absolute T2, and PpIX fluorescence are all significant (black asterisks) from the controls. The GFP + ROIs are further broken down into groups of H&E + ROIs (c) and H&E − ROIs (d) to illustrate the large variation between these two groups. The H&E positive ROIs have the same statistically significant groups as all tumor bearing mice, but the H&E negative ROIs are only significant for PpIX fluorescence and T2 map.

Figs. 1(b) and 1(c), respectively, while the MR images are shown in Figs. 1(d)–1(j).

3.2 PpIX Fluorescence and MRI Contrast Comparison

All ROIs were analyzed for PpIX fluorescence, and contrast in the following MR images: T1W, T1W + Gd, T1WCD, T2, T2 map, diffusion, and D_{av} map. The resultant image contrast values are presented in box and whisker plots in Fig. 2. When considering the GFP + ROIs [Fig. 2(b)] the PpIX fluorescence,

T1W + Gd, and T2 Map are all statistically significant from the control ROIs [Fig. 2(a)] at $p < 0.05$. For the H&E + ROIs, the same three imaging types produce statistically significant results as compared to the control ($p < 0.05$). However, when considering only the H&E − ROIs, the PpIX and T2 Map are statistically significant from the control group ($p < 0.05$). The diffusion and D_{av} map did not show any statistical significance in any of the ROI groups.

ROC curves were created for the GFP+ and H&E + ROIs [Figs. 3(a) and 3(b), respectively] for PpIX fluorescence, T1W + Gd and T2 Image. The receiver operating
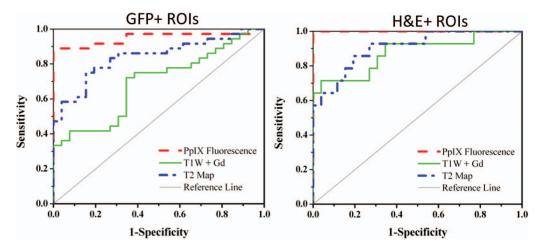

Fig. 3 The ROC curves for the GFP + ROIs (left) and the H&E + ROIs (right) show that PpIX fluorescence has the highest specificity and sensitivity, perfect in the H&E + ROIs case, as compared to the other imaging techniques. The T1W + Gd image contrast is significantly better in the H&E + case, while the T2 map image contrast is relatively similar in both the GFP + and H&E + ROIs. The AUC for each of the image-ROI combination is summarized in Table 1.

Table 1 Diagnostic test results for the three ROI analysis groups: All ROIs, H&E + ROIs and H&E − ROIs.

| Diagnostic tests | Type of imaging contrast | | | | | | | | |
| | All ROIs | | | H&E + ROIs | | | H&E − ROIs | | |
	PpIX	T1W + Gd	T2 map	PpIX	T1W + Gd	T2 map	PpIX	T1W + Gd	T2 map
AUC[a]	0.95 (±0.04)	0.69 (±0.07)	0.84 (±0.05)	1 (±0)	0.88 (±0.05)	0.91 (±0.05)	0.91 (±0.05)	0.55 (±0.09)	0.79 (±0.07)
Sensitivity	0.89	0.28	0.64	1	0.57	0.71	0.82	0.09	0.59
Specificity	1	1	0.85	1	1	0.85	1	1	0.85
PPV[a]	1	1	0.81	1	1	0.82	1	1	0.79
NPV[a]	0.90	0.58	0.70	1	0.70	0.75	0.85	0.52	0.67
Diag. Acc.[a]	0.94	0.64	0.74	1	0.79	0.78	0.91	0.55	0.72

[a]AUC = area under the curve (refers to ROC curves in Figure 3), PPV = positive predictive value, NPV = negative predictive value, Diag. Acc. = diagnostic accuracy.

characteristic (ROC) curves demonstrate the relationship between the false positive fraction and the true positive fraction based on the image contrast, as compared to the contrast in the control mice. PpIX fluorescence image contrast displays the highest sensitivity and specificity of the three imaging types in both GFP + and H&E + ROI groups, with perfect scoring for the H&E + ROIs. T1W + Gd image contrast displays higher sensitivity in the H&E + ROI group than that in the GFP + ROI group and has similar specificities. The T2 map exhibits similar sensitivity and specificity in both GFP + and H&E + ROI groups.

The area under the curve (AUC) for each ROC curve image type is summarized in Table 1 and describes how accurately the tumor can be differentiated from the control; where an area of 1 indicates 100% sensitivity and specificity, while an area of 0.5 is indicative of 50% sensitivity and specificity, or random guessing. The AUCs for the H&E + ROI group are all higher than the AUCs for the GFP + ROI group, although the individual imaging contrast types all show the same trends with PpIX fluorescence > absolute T2 > T1W + Gd. The H&E − ROI group shows a high level of false positives for the PpIX fluorescence and absolute T2, while the T1W + Gd is close to the control group.
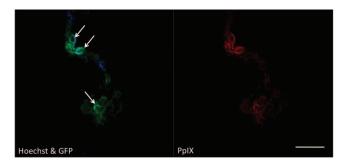
A complete summary of diagnostic tests is provided in Table 1. The results of the diagnostic tests demonstrate the same basic trends as seen for the AUC. PpIX image contrast is consistently higher in sensitivity, NPV, and diagnostic accuracy for all three ROI groups. T1W + Gd image contrast also shows perfect specificity and PPV for all three ROI groups; however, T1W + Gd has lower NPV and diagnostic accuracy values than PpIX. In fact, T1W + Gd has lower sensitivity, NPV, and diagnostic accuracy values than T2 Map.

Correlations between PpIX fluorescence and both T1WCD and T2 maps were identified. Pearson's correlation coefficients were 0.79 ($p < 1 \times 10^{-8}$) and 0.74 ($p < 0.003$) for PpIX fluorescence and T1W + Gd image contrast for the GFP + and the H&E + ROIs, respectively, demonstrating highly significant positive linear correlation between PpIX fluorescence and gadolinium enhancement. The Pearson's correlation coef-

ficient for PpIX fluorescence and absolute T2 image was 0.34 ($p < 0.05$) for the GFP + ROI group, indicating a weak positive correlation. No correlation was found between PpIX fluorescence and absolute T2 image in the H&E + ROI group, and no significance was found between PpIX fluorescence and any MR image type in the H&E − ROI group.

3.3 Ex vivo Fluorescence Imaging of Frozen Tissue

Ex vivo fluorescence imaging of frozen brain tissue sections displayed co-localized regions of GFP, Hoechst 33258, and PpIX fluorescence (Fig. 4). The GFP fluorescence channel had some bleed through of the Hoechst 33258 due to the overlapping spectra in the 480 to 560 nm region. Therefore, the GFP and Hoechst 33258 fluorescence images were overlaid and regions of overlap were indicated to distinguish Hoechst 33258. The PpIX fluorescence corresponded well with both the tumor cells (GFP fluorescence) and with perfusing vasculature (Hoechst 33258 fluorescence), but was not observed elsewhere in the brain.

Fig. 4 *Ex vivo* fluorescence imaging of frozen tissue sections confirms the co-localization of GFP (green, left image), perfusing blood vessels (Hoechst, blue, left image), and PpIX fluorescence (red, right image). Due to the nature of the filter, some Hoechst fluorescence leaked into the GFP channel; therefore, these regions are marked with white arrows and indicate areas that contain fluorescence from both the green and blue fluorescence channels and can be attributed to perfusive blood vessels. Scale bar = 200 μm.

4 Discussion

Infiltrative tumors are difficult to detect *in vivo* using MR imaging, especially at the tumor margins where extended growth into normal tissue is occurring. A surgeon using ALA-PpIX FGR needs to rely on the accuracy of the PpIX fluorescence arising from outside of the tumor boundary determined by conventional gadolinium enhanced MR imaging.[7,19] There arises a need to study the correlation of PpIX fluorescence with contrast enhanced MR imaging for the safe removal of all malignant tissues. We have studied *ex vivo* PpIX fluorescence image contrast in comparison to the gold-standard gadolinium enhanced *in vivo* MR imaging, as well as commonly used endogenous MR contrasts in order to identify whether all observed PpIX fluorescence can be classified as malignant tissue. In this case, a human glioma cell line, transfected with green fluorescent protein, was used as an infiltrative tumor model. This tumor line was established in house and showed atypical diffuse, infiltrative morphology upon orthotopic implantation as compared to the U251 parent line.[15] The parent line displays typical glioma growth patterns in which the tumor is observed as a solid ball within the normal brain tissue. The diffusive nature of the U251-GFP tumor line behaves similarly to the boundaries observed in the parent U251 tumor (and typical of invasive gliomas) where there is a significant amount of infiltrative tumor satellites within the normal tissue.

The diffuse nature of the U251-GFP tumor made it difficult to section successfully as there were many clusters of cells throughout the brain tissue. Originally, a single 4-μm slice was taken from the surface of the brain tissue sections that had been subjected to fluorescence imaging. These H&E surface slices did display tumor cells corresponding to the GFP fluorescence; however, there were many regions that displayed GFP fluorescence that were not found in the surface H&E section. The brain slices used for GFP fluorescence collection were several millimeters thick, and were not accurately represented by the surface H&E section as fluorescence imaging allows deeper penetration of light into the tissue than the representative 4 μm H&E slice. Therefore, further tissue sections were taken every 100 μm throughout the entirety of the brain. Unfortunately, there were still GFP+ ROIs that were not identified in H&E; likely there were small clusters of tumor cells in the 100 μm of tissue between H&E stained sections that were missed. The diffuse nature of the U251-GFP tumor line often results in only a few cells found in small satellites or clusters [Fig. 1(a)]. Additionally, there were several GFP+ ROIs that corresponded to the ventricles or outer edges of the brain (i.e., in the cerebrospinal fluid), and the U251-GFP cells were likely lost in the extraction, washing, and fixation processes. The GFP+ fluorescence arises from a stably transfected U251 cell line; therefore, any observed fluorescence is representative of the presence of the implanted U251-GFP cells. Therefore, the data were analyzed based on all the GFP+ ROIs ($n = 36$), and then subdivided into H&E+ ($n = 14$) and H&E− ($n = 22$) ROIs for further investigation. The H&E− group is analyzed and presented here for thoughtful discussion only, but the results are not overly interpreted.

The results show that all groups (GFP+, H&E+ and H&E− ROIs) have significant PpIX fluorescence ($p \ll 0.001$) and absolute T2 image ($p \ll 0.01$) contrast as compared to the nontumor control groups, while only the GFP+ ROIs and H&E+ ROIs display significant T1W+Gd contrast ($p < 0.01$). No other MR image type showed significant contrast when

compared to the control using unequal variance two-tailed t-test. PpIX image contrast provides the highest diagnostic accuracy for all three of the ROI groups and displays perfect scores in all diagnostic tests for the H&E+ ROI group (Table 1). Although T1W+Gd shows perfect specificity and PPV but has the lowest NPV for each ROI group, indicating that if used alone, it would be a poor predictor of infilatrative glioma. T2 map has lower specificity and PPV than T1W+Gd but displays higher sensitivity and NPV, therefore providing higher diagnostic accuracy.

Recently, Roberts et al.[7] published a study that compared intraoperative PpIX fluorescence, preoperative MR image features, and neuropathological parameters in glioblastoma multiform patients. It was found that tissues displaying PpIX fluorescence observed by the surgeon had significantly higher Gd enhancement (here called T1WCD) and normalized contrast ratio ($nCR = [I_{ROI} − I_{Contra}]/I_{Bkgd}$, where each intensity represents the average voxel intensity of that region) values than tissues without PpIX fluorescence. Although similar to our results, the T1WCD images in this study did not display a statistical difference from the control groups due to the very large standard deviation in the results; however, it is important to note that had an equal variance two-tailed t-test been performed, the T1WCD image group would have been statistically significant for the GFP+ and H&E+ ROIs. Additionally, the calculation for contrast that was used is slightly different but provides the same result that the T1W+Gd image contrast is significant in malignant gliomas.

A more recent publication from the same group[19] demonstrates that a surgeon's ability to distinguish abnormal tissue from normal based on PpIX fluorescence had a success rate of 0.73 (± 0.03) based on AUC analysis, while true PpIX concentration determined via spectroscopic analysis had a success rate of 0.95 (± 0.02) for all tissues, agreeing with our PpIX image contrast that had an AUC of 0.95 (± 0.04) for all GFP+ ROIs. When we only look at H&E+ ROIs, the predictive power becomes 100%, with an AUC of 1.0, indicating that PpIX has a very strong predictive power for malignant disease.

This study demonstrated a strong Pearson's correlation coefficient, which describes the linearity between samples, when comparing the T1W+Gd and PpIX image contrast within both the GFP+ (0.79, $p < 1 \times 10^{-8}$) and the H&E+ (0.74 $p < 0.003$) ROIs. There is a strong correlation between the amount of gadolinium contrast enhancement in an MR image and the concentration of PpIX produced by the same tissue. To the author's knowledge, this is the first time this has been demonstrated in a glioma model, and is likely due to the breakdown of the BBB in the tumor region allowing high levels of accumulation for both ALA and gadolinium. Tynninen et al.[18] showed a correlation between both microvessel density and histological cell proliferation and increased enhancement in Gd-enhanced MR imaging.

There was no significant difference of the T1W+Gd image contrast for the H&E− groups, and therefore did not correlate with the observed PpIX production. This is likely due to one of two things: 1. the size of the tumor satellite/clusters were too small (hence, they were missed in the serial H&E sections) and had not yet been vascularized; or 2. the PpIX arising from these ROIs cannot be attributed to malignant glioma tissue. Magnevist®, the gadolinium contrast agent used here,

is more than five times larger than ALA, limiting diffusion in BBB protected areas. Olivo and Wilson also noted that ALA can cross the BBB, so that PpIX accumulation in small tumor clusters is a reasonable estimate of what occurred here.[13] However, the same authors also observed that PpIX production within the brain could be from another source such as inflammation,[13] radiation necrosis,[19] and neurodegenerative disease associated with inflammation.[19] Since GFP fluorescence was observed in these ROIs, it is possible that these were small U251-GFP clusters with no, or very limited, BBB breakdown.

5 Conclusions

This study shows that both *in vivo* standard gadolinium contrast enhanced and absolute T2 MR images can positively predict the presence of diffuse gliomas; however, *ex vivo* PpIX fluorescence accomplishes the same feat with higher sensitivity and diagnostic accuracy. Although the PpIX concentration and gadolinium enhancement are linearly correlated, there appears to be a limit on the ability of MR to detect these diffuse gliomas, likely due to tumor cell cluster size or amount of BBB breakdown. ALA-PpIX–based FGR has great promise for complete a resection of gliomas, especially if the surgeon is confident in the PpIX fluorescence signal within tumor margins and in cases of diffusely spread tumors. Thinking broadly about the variation in image quality between systems and hospitals, it is always possible to obtain sub-standard image quality; thus, having two systems that work together to provide redundant and also synergistic data for higher sensitivity and specificity will be critical. It seems likely that the combined use of pre-operative MRI, together with fluorescence imaging during surgery, would be the most effective way to guide glioma resection.

References

1. W. Stummer, A. Novotny, H. Stepp, C. Goetz, K. Bise, and H. J. Reulen, "Fluorescence-guided resection of glioblastoma multiforme by using 5-aminolevulinic acid-induced porphyrins: a prospective study in 52 consecutive patients," *J. Neurosurg.* **93**(6), 1003–1013 (2000).
2. W. Stummer, U. Pichlmeier, T. Meinel, O. D. Wiestler, F. Zanella, H. J. Reulen, and for the ALA-Glioma Study Group, "Fluorescence-guided surgery with 5-aminolevulinic acid for resection of malignant glioma: a randomised controlled multicentre phase III trial," *Lancet Oncol.* **7**(5), 392–401 (2006).
3. W. Stummer, H. J. Reulen, T. Meinel, U. Pichlmeier, W. Schumacher, J. C. Tonn, V. Rohde, F. Oppel, B. Turowski, C. Woiciechowsky, K. Franz, and T. Pietsch, "Extent of resection and survival in glioblastoma multiforme: identification of and adjustment for bias," *Neurosurgery* **62**(3), 564–576 (2008).
4. W. Stummer, H. J. Reulen, A. Novotny, H. Stepp, and J. C. Tonn, "Fluorescence-guided resections of malignant gliomas-an overview," *Acta Neurochir [Suppl]* **88**, 9–12 (2003).
5. W. Stummer, H. Stepp, G. Moller, A. Ehrhardt, M. Leonhard, and H. J. Reulen, "Technical principles for protoporphyrin-IX-fluorescence guided microsurgical resection of malignant glioma tissue," *Acta Neurochir.* **140**(10), 995–1000 (1998).
6. W. Stummer, S. Stocker, S. Wagner, H. Stepp, C. Fritsch, C. Goetz, A. E. Goetz, R. Kiefmann, and H. J. Reulen, "Intraoperative detection of malignant gliomas by 5-aminolevulinic acid-induced porphyrin fluorescence," *Neurosurgery* **42**(3), 518–525 (1998).
7. D. W. Roberts, P. A. Valdes, B. T. Harris, K. M. Fontaine, A. Hartov, X. Fan, S. Ji, S. S. Lollis, B. W. Pogue, F. Leblond, T. D. Tosteson, B. C. Wilson, and K. D. Paulsen, "Coregistered fluorescence-enhanced tumor resection of malignant glioma: relationships between delta-aminolevulinic acid-induced protoporphyrin IX fluorescence, magnetic resonance imaging enhancement, and neuropathological parameters," *J. Neurosurg.* **114**(3), 595–603 (2011).
8. P. A. Valdes, X. Fan, S. Ji, B. T. Harris, K. D. Paulsen, and D. W. Roberts, "Estimation of brain deformation for volumetric image updating in protoporphyrin IX fluorescence-guided resection," *Stereotact. Funct. Neurosurg.* **88**(1), 1–10 (2010).
9. P. A. Valdes, K. Samkoe, J. A. O'Hara, D. W. Roberts, K. D. Paulsen, and B. W. Pogue, "Deferoxamine iron chelation increases delta-aminolevulinic acid induced protoporphyrin IX in xenograft glioma model," *Photochem. Photobiol.* **86**(2), 471–475 (2010).
10. P. A. Valdes, F. Leblond, A. Kim, B. T. Harris, B. C. Wilson, X. Fan, T. D. Tosteson, A. Hartov, K. Erkmen, N. E. Simmons, K. D. Paulsen, and D. W. Roberts, "Quantitative fluorescence in intracranial tumor: implications for ALA-induced PpIX as an intraoperative biomarker," *J. Neurosurg.*, ePub ahead of print, **115**, 1–22 (2011).
11. M. Hefti, G. von Campe, M. Moschopulos, A. Siegner, H. Looser, and H. Landolt, "5-aminolevulinic acid induced protoporphyrin IX fluorescence in high-grade glioma surgery: a one-year experience at a single institutuion," *Swiss Medical Weekly* **138**(11–12), 180–185 (2008).
12. S. Collaud, A. Juzeniene, J. Moan, and N. Lange, "On the selectivity of 5-aminolevulinic acid-induced protoporphyrin IX formation," *Curr. Med. Chem.* **4**(3), 301–316 (2004).
13. M. Olivo and B. C. Wilson, "Mapping ALA-induced PPIX fluorescence in normal brain and brain tumour using confocal fluorescence microscopy," *Int. J. Oncol.* **25**(1), 37–45 (2004).
14. D. Croteau, L. Scarpace, D. Hearshen, J. Gutierrez, J. L. Fisher, J. P. Rock, and T. Mikkelsen, "Correlation between magnetic resonance spectroscopy imaging and image-guided biopsies: semiquantitative and qualitative histopathological analyses of patients with untreated glioma," *Neurosurgery* **49**(4), 823–829 (2001).
15. S. L. Gibbs-Strauss, J. A. O'Hara, S. Srinivasan, P. J. Hoopes, T. Hasan, and B. W. Pogue, "Diagnostic detection of diffuse glioma tumors in vivo with molecular fluorescent probe-based transmission spectroscopy," *Med. Phys.* **36**(3), 974–983 (2009).
16. S. C. Davis, K. S. Samkoe, J. A. O'Hara, S. L. Gibbs-Strauss, H. L. Payne, P. J. Hoopes, K. D. Paulsen, and B. W. Pogue, "MRI-coupled fluorescence tomography quantifies EGFR activity in brain tumors," *Acad. Radiol.* **17**(3), 271–276 (2010).
17. S. Mori and P. C. M. Van Zijl, "Diffusion weighting by the trace of the diffusion tensor within a single scan," *Magn. Reso. Med.* **33**(1), 41–52 (1995).
18. O. Tynninen, H. J. Aronen, M. Ruhala, A. Paetau, K. Von Boguslawski, O. Salonen, J. Jääskeläinen, and T. Paavonen, "MRI enhancement and microvascular density in gliomas: correlation with tumor cell proliferation," *Invest. Radiol.* **34**(6), 427–434 (1999).
19. S. Miyatake, T. Kuroiwa, Y. Kajimoto, M. Miyashita, H. Tanaka, and M. Tsuji, "Fluorescence of non-neoplastic, magnetic resonance imaging-enhancing tissue by 5-aminolevulinic acid: case report," *Neurosurgery* **61**(5), E1101–1103; discussion E1103-1104 (2007).